Technical University of Denmark

DTU

Theory for upconversion of incoherent images

Dam, Jeppe Seidelin; Pedersen, Christian; Tidemand-Lichtenberg, Peter

DTU Library
Technical Information Center of Denmark

Theory for upconversion of incoherent images

Jeppe Seidelin Dam,* Christian Pedersen, and Peter Tidemand-Lichtenberg

DTU Fotonik, Department of photonics engineering, Technical University of Denmark, DK-4000 Roskilde, Denmark
*jdam@fotonik.dtu.dk

Abstract: Upconversion of images is a generic method for shifting the spectral content of entire images. A comprehensive theory for upconversion of incoherent light images is presented and compared against experiments. In particular we consider the important case for upconversion of infinity corrected light. We show that the spatial resolution for upconversion of incoherent light images is better than for the corresponding coherent image upconversion case. The fundamental differences between upconversion of coherent and incoherent images are investigated theoretically and experimentally. The theory includes the general case of upconversion using TEM_{nm} modes.

©2012 Optical Society of America

References and links

1. J. E. Midwinter, "Image conversion from 1.6 μ to the visible in lithium niobate," Appl. Phys. Lett. **12**(3), 68–70 (1968).
2. J. Warner, "Spatial resolution measurements in up-conversion from 10.6 m to the visible," Appl. Phys. Lett. **13**(10), 360–362 (1968).
3. J. F. Weller and R. A. Andrews, "Resolution measurements in parametric upconversion of images," Opt. Quantum Electron. **2**(3), 171–176 (1970).
4. R. W. Boyd and C. H. Townes, "An infrared upconverter for astronomical imaging," Appl. Phys. Lett. **31**(7), 440–442 (1977).
5. R. A. Andrews, "IR image parametric up-conversion," IEEE J. Quantum Electron. **6**(1), 68–80 (1970).
6. A. H. Firester, "Image Upconversion: Part III," J. Appl. Phys. **41**(2), 703–709 (1970).
7. J. Falk and W. B. Tiffany, "Theory of parametric upconversion of thermal images," J. Appl. Phys. **43**(9), 3762–3769 (1972).
8. K. F. Hulme and J. Warner, "Theory of thermal imaging using infrared to visible image up-conversion," Appl. Opt. **11**(12), 2956–2964 (1972).
9. W. Chiou, "Geometric optics theory of parametric image upconversion," J. Appl. Phys. **42**(5), 1985–1993 (1971).
10. F. Devaux, A. Mosset, E. Lantz, S. Monneret, and H. Le Gall, "Image Upconversion from the Visible to the UV Domain: Application to Dynamic UV Microstereolithography," Appl. Opt. **40**(28), 4953–4957 (2001).
11. P. M. Vaughan and R. Trebino, "Optical-parametric-amplification imaging of complex objects," Opt. Express **19**(9), 8920–8929 (2011).
12. J. S. Dam, C. Pedersen, and P. Tidemand-Lichtenberg, "High-resolution two-dimensional image upconversion of incoherent light," Opt. Lett. **35**(22), 3796–3798 (2010).
13. S. Baldelli, "Sensing: Infrared image upconversion," Nat. Photonics **5**(2), 75–76 (2011).
14. C. Pedersen, E. Karamehmedović, J. S. Dam, and P. Tidemand-Lichtenberg, "Enhanced 2D-image upconversion using solid-state lasers," Opt. Express **17**(23), 20885–20890 (2009).
15. M. J. Missey, V. Dominic, L. E. Myers, and R. C. Eckardt, "Diffusion-bonded stacks of periodically poled lithium niobate," Opt. Lett. **23**(9), 664–666 (1998).
16. J. Hellström, V. Pasiskevicius, H. Karlsson, and F. Laurell, "High-power optical parametric oscillation in large-aperture periodically poled KTiOPO(4)," Opt. Lett. **25**(3), 174–176 (2000).

1. Introduction

Upconversion of infrared images has been explored by several authors as a possible method for infrared imaging [1–4]. In the 1970's several papers describing the theory of image upconversion were published [5–9]. In those papers the theory for upconversion of incoherent light images was presented in a very complex and general formulation. Different conclusions came out the early work; one important finding of the work in [9] is that aberrations caused by finite thickness of the nonlinear crystal vanish for mixing with infinity corrected light. In [8]

the predicted continuous wave (cw) quantum efficiencies were limited to $5.5 \cdot 10^{-7}$, and experimentally demonstrated cw quantum efficiencies never exceeded $2 \cdot 10^{-7}$ [4]. While little research has been done on cw image upconversion in recent years, there has been work based on pulsed lasers [10, 11]. For upconversion of stationary incoherent emitting or illuminated objects there is no advantage in using pulsed lasers, since the converted signal can be no better than what could be obtained with the same average power in cw operation. However, pulsed systems might be preferred in experiments where the radiation has fast or periodic temporal variations then a pulsed mixing laser can act as a time-gate. Pulsed upconversion could also be relevant in systems where a pulsed incoherent light source is used, e.g. pump probe experiments.

Recently, we experimentally demonstrated high resolution upconversion of near infrared incoherent light, showing three orders of magnitude improvement in both resolution and quantum efficiency [12], when compared to prior art cw image upconversion [4]. This led to the principle being put forward as a feasible method for infrared imaging [13]. Very high quantum efficiency cw upconversion of coherent light has also been shown although with limited resolution [14].

In this paper, a simple theory for image upconversion of incoherent light is derived, following the same principles as for the theory presented for coherent illumination [14]. The derived theory for upconversion of incoherent light will, however, reveal fundamental differences when compared to the coherent case. These differences will be demonstrated theoretically as well as experimentally. In [14] it was shown that high spatial frequency components in a coherent image are not upconverted at all, while in the incoherent case they will contribute to the image formation in blurred form. In the coherent case, this implies that edges of objects are cut away and very small features leave little trace. Furthermore, we show the smallest resolvable features in the incoherent case are $\sqrt{2}$ smaller than the resolvable features in coherent images.

Finally, the theory is for the first time extended to include upconversion using higher order TEM_{nm} modes. Examples of upconversion with higher order TEM_{nm} modes are presented showing the predictive strength of the derived theoretical model. In particular we discuss how such modes may be used to optimize resolution.

2. Theory using a TEM_{00} mode

The theory presented here is based on upconversion of images in a non-linear crystal placed in an infinity corrected plane. This is similar to how modern microscopes work where e.g. filtering is performed in the infinity corrected plane. This approach is beneficial in part to bring about a simple theory, but also for obtaining optimal resolution [3], and further guarantees that no aberrations are caused by the finite length of the non-linear crystal [9].

The theory is derived for upconversion using a Gaussian beam, but subsequently the more general case of higher order Hermite-Gaussian modes is discussed including experimental results.

For upconversion of one wavelength, λ_1, via an intense laser field, λ_2, to the sum frequency generated wavelength, λ_3, energy conservation dictates that the wavelengths are related according to Eq. (1). In this work, we consider a single frequency laser with negligible bandwidth. This infers that the frequency spectrum from the object is shifted by exactly the frequency of the laser.

$$\frac{1}{\lambda_3} = \frac{1}{\lambda_2} + \frac{1}{\lambda_1} \tag{1}$$

The radiation from an incoherently illuminated object or an incoherently (thermally) emitting object can be modeled as a sum of light emitting point sources emitting spherical waves, see Fig. 1. These spherical waves are then transformed to plane waves by a lens placed one focal length, f, from the object plane. Each plane wave is mixed inside the non-linear crystal with a Gaussian laser beam, producing an upconverted field at λ_3 cropped by the

Gaussian beam. This upconverted light is then Fourier transformed by a second lens, f_1, to the image plane producing an upconverted Gaussian spot in the image plane. As will be described in the following, this Gaussian spot is the point spread function of the image upconversion system.

Since the object light is incoherent (has random phase components), the corresponding upconverted light is also incoherent, i.e. random phase distribution. For this reason, only the intensities and spectral radiances are considered in the following. Thus, the point spread function "acts" on the intensities or radiance, rather than on the electric field as is the case in coherent image upconversion [14].

Radiation from incoherent light sources, e.g. blackbodies, is usually described in terms of spectral radiance, unlike in laser physics where terms as intensities and electric fields are usually preferred. While the following calculations could be done with intensities and electric fields, the calculations turn out much simpler when considering radiances.
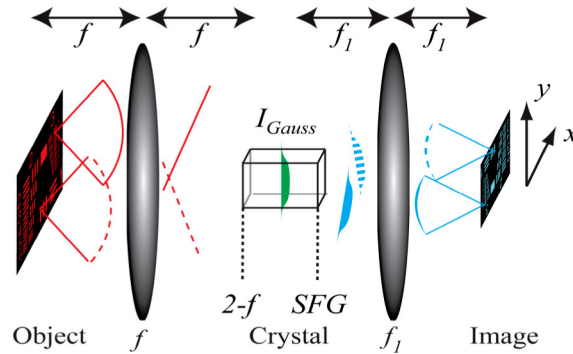

Fig. 1. An object is emitting incoherent light, which can be modeled as points emitting spherical waves. A lens, f, transforms these spherical waves to plane waves. The plane waves are cropped by an on-axis Gaussian upconverting beam and shifted to a different wavelength. These waves exit the non-linear crystal at a smaller angle due to momentum conservation. The individually upconverted Gaussian waves forms an image after a lens, f_1, and must be added incoherently (as intensities) in the image plane.

Starting from the image plane, the first step in the optical system is the image formation performed by the lens f_1. Note that the spectral radiance, L, is conserved in (lossless) geometrical optics. Thus, the spectral radiance in the image, L_{Image}, is conserved from the spectral radiance at the output of the non-linear crystal, L_{SFG}. In the setup, a position in the image plane (x, y) corresponds to an angle $(x / f_1, y / f_1)$ at the output of the nonlinear crystal. Likewise, angles (θ, ϕ) in the image plane relate to positions $(-\theta f_1, -\phi f_1)$ in the SFG plane, Eq. (2).

$$L_{Image}\left(x, y, \theta, \phi, \lambda_3\right) = L_{SFG}\left(-\theta f_1, -\phi f_1, \frac{x}{f_1}, \frac{y}{f_1}, \lambda_3\right) \qquad (2)$$

This relation is used extensively in the following. Since all angles in the imaging are small, a paraxial approximation is used.

L_{Object} is the spectral radiance at the object plane and is assumed to be composed of incoherent point sources. Point sources are by definition spherical emitters, and thus L_{Object} will only be a function of position and wavelength. Consequently, the radiance at the crystal input plane L_{2-f} is constant in transverse position, i.e. a plane wave.

Next, the spectral radiance at the output of the nonlinear crystal, L_{SFG}, is related to the spectral radiance at the input of the crystal, L_{2-f}, through the non-linear conversion process. We note that due to momentum conservation in the upconversion process the output angles scale by a factor λ_3/λ_1 compared to the incident angles. Consequently, the spectral radiance increases by $(\lambda_1/\lambda_3)^2$. The nonlinear interaction inside the crystal is assumed small, i.e. the small signal approximation can be applied. Furthermore, collinear interaction between the

waves is considered. The upconverting laser beam is assumed Gaussian distributed, with beam waist w_0 and wavelength λ_2.

With reference to Fig. 1, using geometrical optics and the above listed approximations for the upconversion process, the relationship between the radiance $L_{Image}(x, y, \theta, \phi, \lambda_3)$ in the image plane and the object plane is found as detailed in Eq. (3).

$$
\begin{aligned}
L_{Image}\left(x, y, \theta, \phi, \lambda_3\right) &= L_{SFG}\left(-\theta f_1, -\phi f_1, \frac{x}{f_1}, \frac{y}{f_1}, \lambda_3\right) \\
&= C \cdot sinc^2\left(\frac{\Delta k l}{2}\right) \cdot I_{Gauss}\left(-\theta f_1, -\phi f_1, \lambda_2\right) \cdot \left(\frac{\lambda_1}{\lambda_3}\right)^2 \cdot L_{2-f}\left(\frac{\lambda_1}{\lambda_3}\frac{x}{f_1}, \frac{\lambda_1}{\lambda_3}\frac{y}{f_1}, \lambda_1\right) \\
&= C \cdot sinc^2\left(\frac{\Delta k l}{2}\right) \cdot I_{Gauss}\left(-\theta f_1, -\phi f_1, \lambda_2\right) \cdot \left(\frac{\lambda_1}{\lambda_3}\right)^2 \cdot L_{Object}\left(-\frac{\lambda_1}{\lambda_3}\frac{f}{f_1}x, -\frac{\lambda_1}{\lambda_3}\frac{f}{f_1}y, \lambda_1\right)
\end{aligned}
\tag{3}
$$

Where the non-linear conversion efficiency is given as: $C = \dfrac{8\pi^2 d_{eff}^2 l^2}{n_1 n_2 n_3 \varepsilon_0 c \lambda_3^2}$.

ε_0 is the vacuum permeability, c is the speed of light in vacuum, d_{eff} is the effective nonlinear coefficient of the crystal, l is the length of the crystal, n_i is the refractive index corresponding to wavelength λ_i. $\Delta k = k_3 - k_2 - k_1$, where k_i is the k-vector corresponding to the three waves. $I_{Gauss}(-\theta f_1, -\phi f_1, \lambda_2)$ is the Gaussian intensity distribution of the laser beam. It is noted that (θ, ϕ) do not enter the expression for L_{object}, since we assume that light is emitted uniformly in all directions. Consequently, L_{2-f} is independent of transverse position (plane wave).

The last step involves rewriting of the image radiance, L_{Image}, into an intensity distribution, I_{Image} and to include diffraction caused by the Gaussian cropping inside the nonlinear crystal.

To obtain the intensity at the image plane, integration over angles, (θ, ϕ), is performed. Since the upconverted light from a single point in the object plane is Gaussian distributed when exiting the upconversion crystal, the diffraction can be described by a Fourier transform of the Gaussian intensity distribution. This gives the point spread function. Note, that this step is analog to the imaging process through a Gaussian aperture. Thus, the blurring of the image can be accurately described by a Gaussian convolution, Eq. (4).

$$
\begin{aligned}
I_{Image}\left(x, y, \lambda_3\right) &= \frac{8\pi^2 d_{eff}^2 l^2 sinc^2\left(\frac{\Delta k l}{2}\right)}{n_1 n_2 n_3 \varepsilon_0 c \lambda_3^2} \cdot P_{Gauss} \cdot \left(\frac{\lambda_1}{f_1 \lambda_3}\right)^2 \cdot \\
&\quad L_{Object}\left(-\frac{\lambda_1}{\lambda_3}\frac{f}{f_1}x, -\frac{\lambda_1}{\lambda_3}\frac{f}{f_1}y, \lambda_1\right) \otimes \left(\frac{2\pi w_0^2}{(\lambda_3 f_1)^2} e^{-\frac{2(x^2+y^2)\pi^2 w_0^2}{(\lambda_3 f_1)^2}}\right)
\end{aligned}
\tag{4}
$$

P_{Gauss} is the power of the laser beam.

Since the derived theory is concerned with the incoherent case, the point spread function acts on the intensity, rather than the electric field in contrast to coherent upconversion [14].

It is important to note, that the upconverted image intensity is completely independent of the beam size, w_0. The mixing laser beam size exists only as a part of the normalized convolution function which relates to resolution of the image. Since the convolution function approaches a delta function as w_0 increases, the conclusion is clear: The upconverted intensity is independent of beam waist size w_0 of the mixing laser field. The convolution function can be regarded as the imaging point spread function (PSF). The optical transfer function (OTF) is the Fourier transform of the PSF. This means that the laser beam shape inside the crystal defines the OTF.

Another interesting feature is that Eq. (4) is not a function of f, except as a magnification factor of the image. This is also in contrast to the coherent case [14].

Equation (4) is valid only when the upconverted light can be considered collinear with the intracavity laser field. This can be approximately quantified as the angle of the upconverted light, λ_3, being smaller than w_0 / l. Beyond this limit, the upconversion still works, but the modeling of the imaging properties require a more comprehensive theory to be developed. Furthermore, the phase matching condition, Δk, is a function of propagation angles (x / f_1, y / f_1) and refractive indices. The angular dependence of Δk is of second order, which shows that close to the optical axis there will only be small variations from $\Delta k = 0$. At larger angles (the edges of the image) the optimally upconverted wavelength will change. For a 10 mm long PP-LN crystal the typical angular acceptance (intra-crystal) is about 1°, outside this solid angle the phase-matched wavelength will change significantly.

The convolution in Eq. (4) relates to intensity, rather than the E-field (in contrast to coherent image up-conversion [14]). This has direct influence on the achievable resolution, since the e^{-2} diameter is $1/\sqrt{2}$ narrower than for the E-field. Thus the spatial resolution of incoherent image upconversion is $\sqrt{2}$ better than for the corresponding coherent case.

Equation (4) is composed of several components. In fact, it can be split into a term for power conversion efficiency, a term for magnification of the image, and lastly a term for the point spread function. The maximum quantum efficiency (QE_{max}) is found for phase matched light travelling along the center of the nonlinear crystal, Eq. (5).

$$QE_{max} = C \cdot I_{Gauss}(0,0) \cdot \frac{\lambda_3}{\lambda_1} = \frac{16\pi d_{eff}^2 l^2 P_{Gauss}}{n_1 n_2 n_3 \varepsilon_0 c \lambda_1 \lambda_3 w_0^2} \tag{5}$$

The conversion quantum efficiency reference [12] was estimated to be 0.02% whereas according to Eq. (5) theoretically it should have been 0.7%, using an effective non-linearity of $d_{eff} = 11$ pm/V (PP:KTP). This difference can be explained by imperfect periodic poling, since the poling period is quite short (7.2 µm) and the crystal quite thick (1 mm).

3. Comparison of upconversion of coherent and incoherent images

In this section, the differences in upconversion of coherent and incoherent radiation are demonstrated. In order to show the predictive power of the presented theory, experimentally obtained and theoretically calculated results are compared. The first test case is upconversion of the cross used in a previous publication [14]. The cross is illuminated either by a collimated beam from a 766 nm single mode fiber coupled laser (coherent case), or by a halogen microscope light source equipped with a red bandpass filter. The object field is focused into a 10 mm long Brewster-cut intracavity periodically poled KTP crystal by a lens with a focal length of 60 mm, and upconverted to 488 nm in a 100 µm beam waist in a 1342 nm laser. The geometry of the laser has been modified as compared to the setup used in [14]. The result of these experiments can be seen in Fig. 2 where they are compared to theoretical calculations.
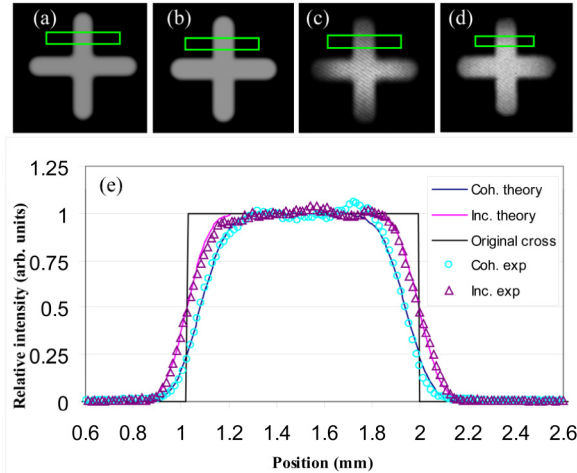
Fig. 2. (a) Theoretical calculation of a coherently illuminated cross. (b) as (a) but for incoherent illumination. (c) Coherent illuminated cross (experiment). (d) Incoherent illuminated cross (experiment). (e) Line traces of theory and experiments. Notice how the coherent crosses appear slimmer and are at a quarter intensity (half E-field) at the intersection with the actual cross.

To further demonstrate the different behaviour for high resolution patterns for conversion of coherent and incoherent images, the converted images from a standard resolution target is considered. The images are calculated using the theoretical point spread function from Eq. (4), with parameters as measured in the previous publication [12]. This is compared to a zoomed in version of the experimentally obtained image from [12] in Fig. 3.
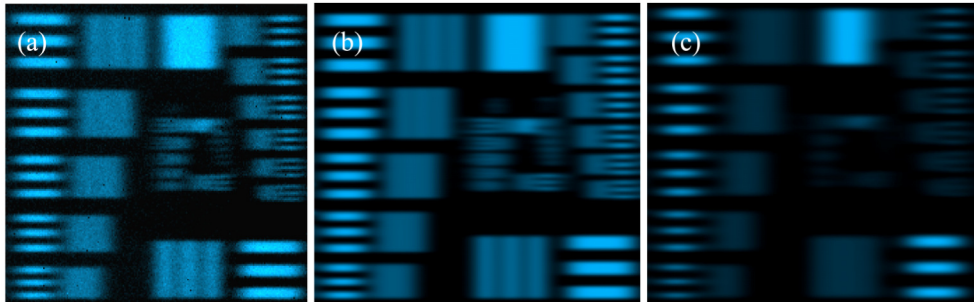

Fig. 3. (a) Experimentally obtained image (incoherent), from [12]. (b) Theoretically calculated upconverted image (incoherent). (c) Theoretically upconverted image (coherent). Notice that (a) and (b) are very similar except for the shot noise. The coherent upconversion, using the same parameters shows the expected poorer resolution as previously calculated. Notice further how the finer features are dimmed considerably in the coherent upconversion case.

Another distinct difference between incoherent and coherent upconversion is tolerances toward misalignment of the imaging system. In [14] it is shown how transverse misalignment of the coherently illuminated object gives rise to different forms of spatial high pass filtering, thus giving a strongly distorted image. In contrast, misalignment in the incoherent case gives practically no distortion at all. The reason can be understood from Fig. 1. Since light from an object point is transformed into a plane wave, filling out the aperture of the nonlinear crystal, a transverse displacement of the emitter from the object does not lead to any appreciable change. Thus, the overlap between the object light and the intracavity beam remains unchanged. In the coherent case the strongly confined object beam is very sensitive to the overlap with the intracavity laser beam.

4. Upconversion of incoherent light using higher order TEM_{nm} modes

So far, this paper has considered upconversion with Gaussian beams. However, the theory can be extended to cover higher order Gaussian modes. Using a TEM_{nm} mode in the upconversion process yields the following result for the upconverted image, I_{Image}^{nm}, Eq. (6).

$$I_{Image}^{nm}(x,y,\lambda_3) = \frac{8\pi^2 d_{eff}^2 l^2 \operatorname{sinc}^2\left(\frac{\Delta kl}{2}\right)}{n_1 n_2 n_3 \varepsilon_0 c \lambda_3^2} \cdot P_{Gauss} \cdot \left(\frac{\lambda_1}{f_1\lambda_3}\right)^2 \cdot$$

$$L_{Object}\left(-\frac{\lambda_1}{\lambda_3}\frac{f}{f_1}x, -\frac{\lambda_1}{\lambda_3}\frac{f}{f_1}y, \lambda_1\right) \otimes \left(\frac{2\pi w_0^2}{n!m!2^{n+m}(\lambda_3 f_1)^2} H_n^2\left(\frac{\sqrt{2}\pi w_0}{\lambda_3 f_1}x\right) H_m^2\left(\frac{\sqrt{2}\pi w_0}{\lambda_3 f_1}y\right) e^{-\frac{2(x^2+y^2)\pi^2 w_0^2}{(\lambda_3 f_1)^2}}\right) \tag{6}$$

Where H_j is j'th order Hermite polynomial. Analogous to Eq. (4) the right hand side of the convolution is the point spread function when using a TEM_{nm} mode.

   To experimentally illustrate the effects of upconversion with higher order modes the filament of a light bulb is upconverted using low magnification, so that the filament (for practical purposes) resembles a line. The experimental setup is described in [14]. The higher order modes were created by misalignment of one of the mirrors in the laser cavity and visually identifying the mode order using an IR detector card. The results are shown in Fig. 4.
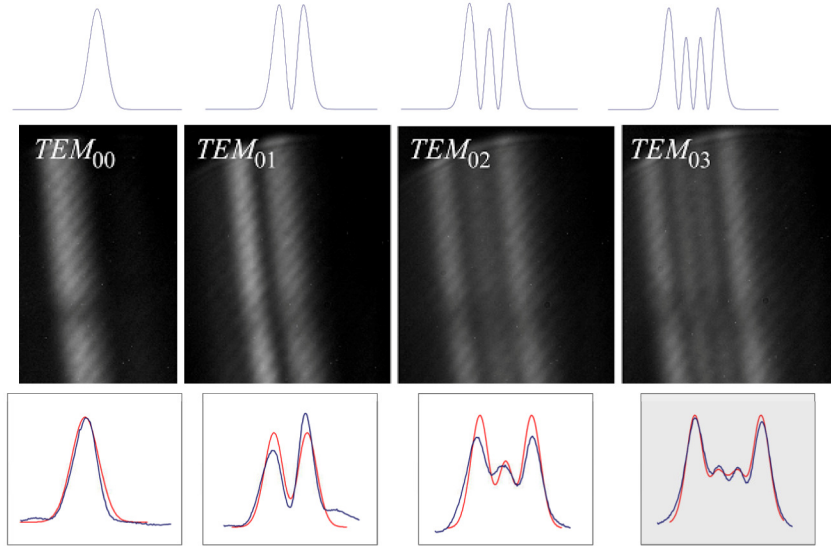

Fig. 4. In this example the result of upconversion of a line source with a Gaussian TEM_{00}, TEM_{01}, TEM_{02}, and TEM_{03} mode respectively, is shown. Sections of the upconverted images are compared to the theoretically predicted images in the lower sets of curves, as modeled from a finite width line source. We note that the central lines in the TEM_{03} appear sharper (narrower) individually, albeit with poorer contrast. The line width can be accurately determined by fitting the measured intensity distribution in the higher order modes, whereas assessing it from the near TEM_{00} is much harder.

   The images in Fig. 4 are acquired with a 10 s integration time on the camera to reduce the shot noise. This is required in this special case since the thin line source is blurred to a comparatively large area resulting in fairly low intensity on the camera. Generally Fig. 4 demonstrates a good agreement between experiments and theory, Eq. (6), using higher order modes in the upconversion process. Some of the discrepancies between calculated curves and experimental curves are due to less than ideal higher order modes, particularly the asymmetry in or the case of TEM_{01} in Fig. 4.

   When considering this experiment as a method to measure an upper limit for the width of the line source, the TEM_{03} gives a significantly lower limit for the width of the line source. A

slightly thicker line source would make the image copies overlap. This experiment can also be interpreted as a direct image of the point spread function.

Figure 5 shows an experimentally obtained upconverted image and the corresponding theoretically predicted image when using a TEM_{01} mode. The resemblance between Fig. 5(a) the experimental image and Fig. 5(b) the theoretical image using incoherent theory is very good, showing many detailed features, underlining the predictive strength of the proposed theory. Figure 5(c) on the other hand, which has been calculated using the coherent theory, shows how the asymmetric electric field of the mixing laser, results in edge detection in the image.
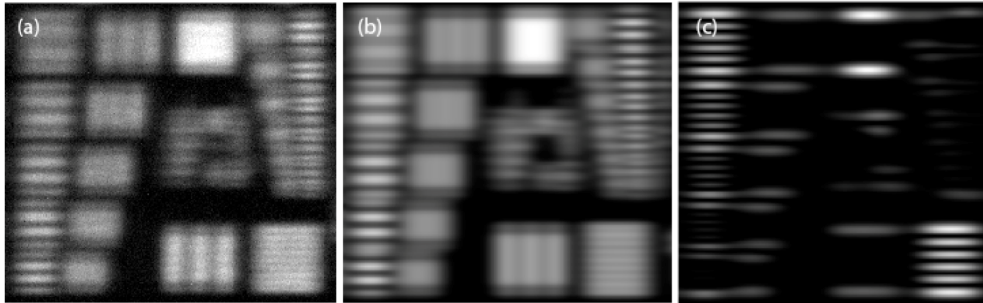

Fig. 5. (a) Experimentally acquired image, and (b) theoretically calculated image based on incoherent theory, (c) shows the upconverted image using coherent theory [14]. All three images use a TEM_{01} laser mode for upconversion.

5. Discussion and outlook

Since the OTF is determined by the shape and size of the laser beam inside the non-linear crystal, the obtainable spatial resolution is ultimately limited by the transverse dimensions of the non-linear crystal. Thus, the obtainable space-bandwidth-product can be increased by using a larger laser beam diameter inside a non-linear crystal with a larger aperture. Periodically poled crystals with large apertures can be designed either by diffusion bonding several identical non-linear crystals into one [15], or by using a non-linear material with low coercive field, allowing for poling of thicker crystals, like possible for KTP [16]. Another straightforward approach is to use a bulk crystal; however, this would limit the design ability of the phase match condition. The edge detection shown possible for coherent light upconversion could be further improved by using doughnut shaped upconversion lasers (Laguerre-Gaussian mode). This would result in an all-optical edge detection scheme.

6. Conclusion

We have derived a simple theory for incoherent image upconversion using Gaussian beams in an infinity corrected setup with good predictive properties as demonstrated experimentally.

The theory of incoherent upconversion displays some interesting and fundamental differences when compared to the coherent case; particularly increased resolution by $\sqrt{2}$ and a power conversion efficiency which is independent of the mixing beam diameter.

We have also demonstrated that the image degradation for the incoherent case is limited to a blurring. For coherent image upconversion, the image degradation is a more significant blurring and the edges and other high spatial frequency components of the images are significantly dimmed.

Finally, we have extended the theory to include higher order Gaussian modes in the upconversion process and experimentally as well as theoretically demonstrated good correlation between theory and experiments when using the proposed infinity corrected setup.